Full Length Research Paper

Application of hyperspectral imaging sensor to differentiate between the moisture and reflectance of healthy and infected tobacco leaves

Babangida Lawal Yusuf* and Yong He

College of Biosystems Engineering and Food Science, Zhejiang University, Hangzhou 310058, China.

The main goal of this research was to develop the real-time remote sensing system as a rapid and field based method of identifying healthy and infected plants at an early stage of disease development, before visibly seen by human eye. This can be achieved through the use of hyper-spectral imaging collected data between 380 to 1030 nm wavelengths. The black-shank disease was inoculated to tobacco plants as a model system for testing this technology. The hypercubes images acquired was processed using ENVI software and the "unscrambler" statistical analysis software for principal components analysis (PCA). Spectral parameter of reflectance sensitivity was used to find the optimal wavelengths for determining and evaluating the level of damage by the black-shank fungus. The result of this research shows that, the spectral reflectance decreases significantly with the increasing severity level in both the visible and near-infrared wavelength ranges. Also the wavelength of 730 and 790 nm with corresponding bands of 283 and 330 was the most useful for discriminating black-shank disease severity level. This research indicates clearly the relationship between spectral properties and plant response.

Key words: Hyperspectral, image processing, moisture, reflectance, tobacco plants, black-shank.

INTRODUCTION

The hyperspectral imaging sensor originally developed for mining and geology to identify various minerals, this make it ideal for the mining and oil industries where it can be used to look for iron-ore and oil. It is now spread into the fields of Agriculture, Ecology, surveillance, pharmaceuticals, historical manuscript research and so on (Glaber et al., 2011). Hyperspectral sensors have been built with capability to collects and process the information from across the electromagnetic spectrum and divide it into many bands. This technique of dividing images into bands can be extended beyond the visibility of human eyes (that is, visible light in three bands of red, green and blue). The collected information is a set of images and each image represents a range of the electromagnetic spectrum (also known as a spectral band). These images are then combined and form a three-dimensional hyperspectral data cube for processing and analysis (Garcia et al., 2008).

The acquired data can be extracted, reduced or compressed using methods such as Principal component analysis (PCA) and independent component analysis (ICA). PCA method used to produce uncorrelated output bands, to segregate noise components, and to reduce the dimensionality of data sets. This is done by finding a new set of orthogonal axes that have their origin at the data mean and that are rotated so the data variance is maximized (Sankaran et al., 2010). ICA use to transform set of mixed and random signals into components that are mutually independent. Independent component transformation serves as a tool for blind source separation, where no prior information on the mixing is available. The transform is based on the non-Gaussian assumption of the independent sources, and uses higher-order statistics to reveal interesting features in typically non-Gaussian hyperspectral datasets (Plaza et al., 2009).

In recent development, hyperspectral imaging improved the use of information available in the reflectance region

_____

*Corresponding author. E-mail: byingawa@yahoo.com. Tel: 0086-571-88982143, 86971143. Fax: 0086-571-86971143.
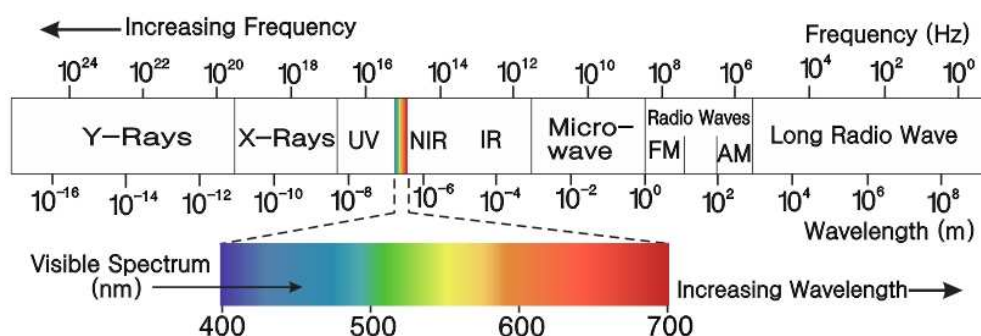
Figure 1. Location of visible spectrum wavelength range in nanometers (nm) from 400 to 700 within Range of Electromagnetic spectrum. Source: http://en.wikipedia.org/wiki/File:EM_spectrum.svg (with permission), accessed 6th Sep, 2011.

of the spectra in combination with image processing software (Brantley et al., 2011). Figure 1 shows the visible spectrum (400 to 700 nm), which is the portion of the electromagnetic spectrum range that can be detected by the human eye in three bands of red, green and blue light. Both the visible spectrum region, near-infrared (NIR), and IR in hyperspectral imaging are used to detect the chemical composition of plants, to determine the nutrient and water status, and estimate the pigment content of leaves such as chlorophyll and carotenoid quantitative determinations (Dian et al., 2008). Hyperspectral method provides high-quality spectral information on the pigment distribution within leaves; through this the healthy and infected vegetables leaves and fruits can be easily differentiated by their reflectance intensities. Hyperspectral also can be used for the development and monitoring health of crops, for example to detect vegetables and fruits varieties and develop an early warning system for disease outbreaks (Bauriegel et al., 2011).

An early disease detection system can aid in decreasing losses caused by plant diseases and can further prevent the spread of diseases. Hyperspectral imaging has been used in many researches for disease detection on plants and fruit varieties. For example the hyperspectral data collected from sugarcane leaf reflectance was used to predict sugarcane yellow leaf virus infection for two cultivars. The result showed that, leaf reflectance was effective at predicting sugarcane yellow leaf virus infection with more than 73% accuracy in both of the two cultivars (Grisham et al., 2010). Similarly, the canopy spectral reflectance of tomato plants in a diseased tomato field in Salinas Valley of California was collected. The mapped disease distribution at different stages showed an accurate conformation of late blight occurrence virus in the field. The spectral reflectance of the field samples indicated that the near infrared (NIR) region, especially 700 to 1300 nm, was much more valuable than the visible range (400 to 700 nm) to detect crop disease (Minghua et al., 2003).

Furthermore, healthy wheat kernels and the wheat kernels visibly damaged by *Sitophilus oryzae*, *Rhyzopertha dominica, Cryptolestes ferrugineus*, and *Tribolium castaneum* were scanned using hyperspectral imaging between 1000 to 1600 nm wavelengths. The results are classified with more than 85% accuracy except the kernels damaged by *Tribolium castaneum* with 73.3% accuracy (Singh et al., 2009). Likewise the detection of chilling injury or damage in cucumbers, by which the region of interest spectral features of chilling injured areas showed the reduction of reflectance intensity. This was resulting from chilling treatment at 0oc over the period at post-chilling room temperature storage. A large spectral difference between good, smooth skins and chilling-injured skins occurred in the visible/near-infrared regions of 700 to 850 nm (Yongliang et al., 2005).

The objective of this research is to provide (i) Non-destructive testing technology using Hyperspectral imaging sensor and samples of Tobacco plants at the range of 380 to 1030 nm wavelength. (ii) To investigating the potential of hyperspectral imaging in terms of discriminating between healthy and black-shank infected leaves by quantification of light absorption and reflectance intensities (iii) To determine the moisture content of these samples plants under different conditions of health (iv) To find the wavelength bands at which leaf reflectance was the most responsive to Tobacco plants damage caused by the black-shank disease.

MATERIALS AND METHODS

The following materials were used in these experiments: hyperspectral imaging system, four pots of young tobacco plants, ENVI version 4.7.1 (environment for visualizing images), image processing software for windows by ITT visual information solution, and the unscrambler version 9.7, software for statistical analysis by (Camo software as).

The hyperspectral imaging system

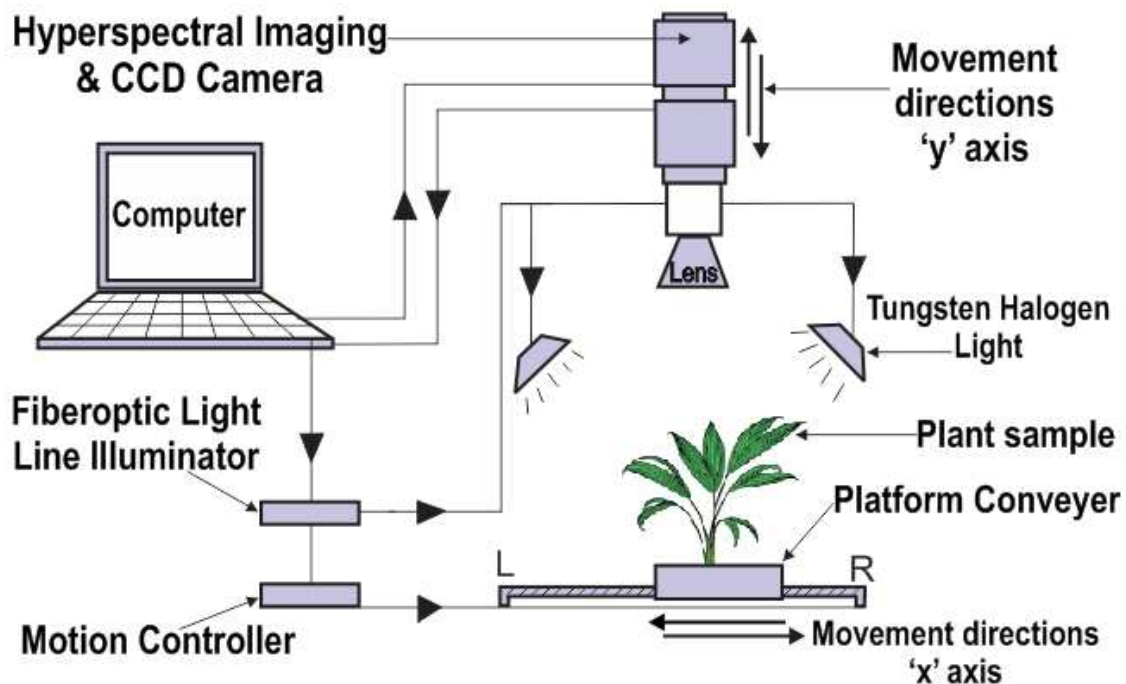Figure 2 shows the diagrammatical representation of Hyperspectral

Figure 2. The hyperspectral imaging system. 'X' axis is indicating movements directions of the conveyer and 'R' is indicating the default position of the conveyer. Data captured only during right to left movement (R—L distance), but during return movement of the conveyer (L—R) no data capture. While the 'Y' axis is indicating the movement directions of the hyperspectral camera were it can be set either to remain stationary, go up or down at specified distance during image capture.

imaging system which was used in these experiments. The system comprises of a Computer with windows operating system, a Hyperspectral imaging camera of wavelength ranges from 380 to 1030 nm (ImSpector V10E, Specim imaging Ltd, Finland), and the field of view (FOV) of 28°. A high-performance CCD camera and Fiber light line illuminator with two pieces 150w tungsten halogen light lamps (Oriel Instruments, USA) set about an angle of 45° each. The user defined speed conveyer which is driven by a stepping motor (Zolix Corp. China, Zolix TS200AB). The enclosure of length, width and height of   (90 × 105 × 180 cm) constructed from sheet metal and columns, providing a rigid platform enclosing all components of the system excluding computer alone.

Hyperspectral system calibrations

During image acquisition there is an electronic current flowing in the detectors or sensors of the CCD arrays even without light shining on it (this current is called electronic dark current or just "dark current). Dark current is dependent on temperature and is proportional to the integration time (Jinsung et al., 2002). It is essential to calibrate the hyperspectral imaging system before acquiring any image or data to ensure the system is operating properly and to diagnose the instrumental errors. In order to get the optimal and satisfied reflectance of the tobacco plants samples, the hyperspectral background spectral response and the dark current image of the CCD camera must be calibrated.

The center and the background reflectance of the hyperspectral were acquired using pure white rectangular-prism ceramics bar, which is one of the hyperspectral accessories with known reflectance of 99% (Naganathan et al., 2008). While for the "dark current image" calibration, the camera lens was completely covered

with its non-transmittance black lid (0% reflectance). These two reference images are used to calculate the pixel-based relative reflectance for the raw line-scan images using Equation 1 (Singh et al., 2009):

$$R = \frac{Ro - D}{W - D} \tag{1}$$

Where R is the relative reflectance image, Ro is the raw reflectance image, D is the dark reference image and W is the white reference image.

Data acquisition and processing

The hyperspectral imaging data is also called Hypercubes, and is built-up as the sensor passes over the ground or over the product, or as the product passing in front of the hyperspectral sensor (Burger and Gowen, 2011). In these experiments, the black background that provides low reflectivity was used in order to avoid much noise and acquire full reflectance of the target object. Figure 3b shows an example of hypercube images acquired from Figure 3a, one of our experimental tobacco plants pots. Also Figure 3(b) shows the hyperspectral data cube structure, which is a 3-dimensional image that comprised of spatial data 'U' and 'V' coordinates, and spectral data created by the diffraction grating which disperses the wavelength of light 'W' (Xu et al., 2008). The hypercube images of the tobacco plants samples was all collected on day 1, 6, 12 and 18 experiments, but without cutting up the leaves from the host plants. Also the room temperature was set to be 21℃ throughout the experiments. All the captured hypercube
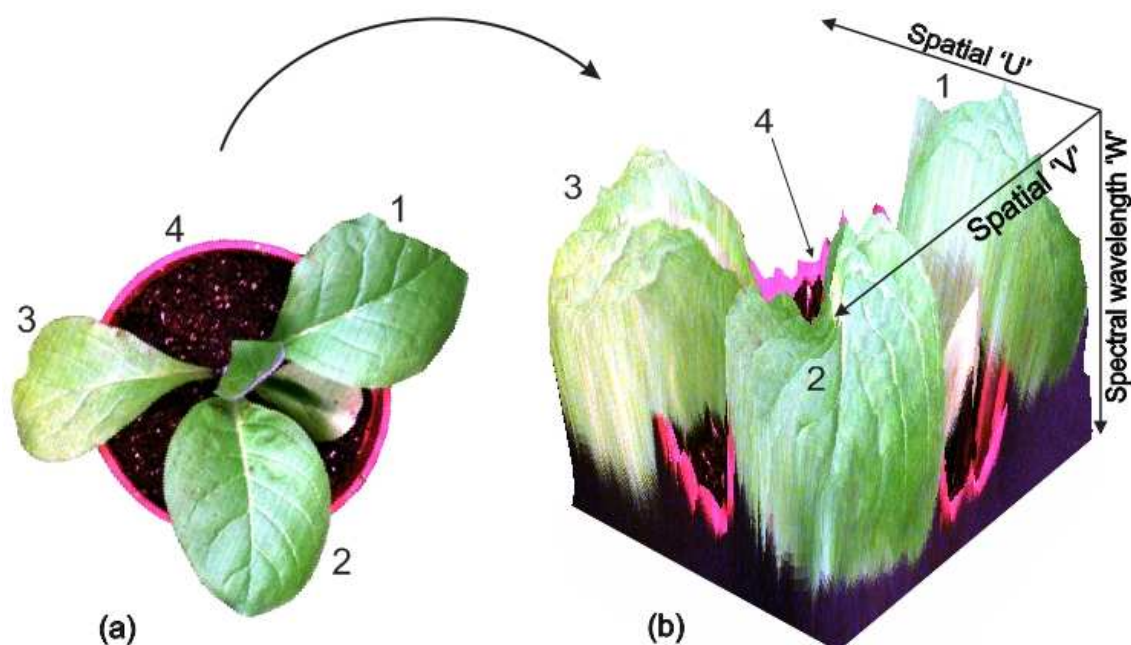
Figure 3. Hyperspectral data structure. Figure 3(b) indicating 3D hyperspectral Image data which is also called 'hypercube data' was acquired from figure 3(a) top view of the Tobacco Plant Pot (RGB images). The spatial axis (U and V) and the spectral wavelength (W) are the lines, samples and spectral bands with the dimensional numbers of (640, 680) and (512) respectively.

images in a raw data format were saved directly into the computer hard disk through the USB port.

Figure 4 shows the spectrometer field of view (FOV), sensor diameter or width, and focal length of the charge-coupled device (CCD) camera. During images shootings the plant samples were conveyed individually to the field of view (FOV) of the hyperspectral imaging. The movement of the conveyer was sets on the speed of 2.5 mm/s up to the distance of 250 mm. This covers the total length of the plants samples, that is, horizontally and X-direction from the hyperspectral software program window. The spectral camera height was adjusted to about 55 cm height above the plant samples, so that the field of view (FOV) was about 25 cm lengths which covered the width of the plants samples. Also the camera remained stationary during images capture, that is, speed in vertical direction from the hyperspectral software program window Y = 0 mm/s (Figure 2).

In order to collect the entire spectral images, the plants were all scanned line-by-line which is also known as push-broom (Naganathan et al., 2008). The estimated image pixel size is 0.35 mm and the sizes in samples, lines and bands of hyperspectral images collected are 640, 680 and 512 respectively. The angle of view, which is used interchangeably with the more general term field of view (FOV), describes the angular extent of a given scene that is imaged by a camera, can be calculated as Equation 2 (Ciaran et al., 2010).

$$FOV = 2 * \arctan \frac{d}{2f} \qquad (2)$$

Where d represents the CCD camera sensor width or diameter, and f is the focal length of the camera (Figure 4).

After acquiring hypercube images and calibrations of reflectance of the tobacco plants samples, three regions in each pot was selected randomly for the first time by selecting boundary areas of a leaf, marked and saved as regions of interest (ROI). The changes of these ROIs (region 1, 2 and 3 at each pot) were monitored throughout the experimental period. Each ROI has covered an average area of 45,000 pixels. Plants were kept in the greenhouse and watered as necessary but no fertilizer was added during 1 to 18 experimental days. Principal component analysis (PCA) was performed to analyse the relationship and differences of healthy and infected plants changes in reflectance and water contents. These were performed by reducing the uncorrelated or principal components (PCs) and maximize representation of the original hyperspectral image data (Muhammed, 2005).

The pot 3 and 4 plants artificial inoculation with black shank pathogen (*Phytophthora nicotianae*) came up immediately after day one experiments. The total of 32 hypercube images was captured and processed using ENVI Image processing Software for windows. During processing of hyperspectral images with ENVI sometimes there is need to specify and assigned the wavelength unit either in micrometers (µm), nanometer (nm), GHz, wavenumber or Index, (if not, error may occur in the result). This can be done from the 'File tab' in the ENVI main menu under 'edit ENVI header' likewise results too can be converted to micrometers, nanometers and so on, 1 mm = 1000 µm, 1 µm = 1000 nm and so on, (Freek, 2004).

Data reduction methods

Principal component analysis (PCA) method

Principal component analysis is a powerful tool for analysing data, also is a variable reduction method that condenses all the spectral information into a few latent variables, which are called principal components (PCs). The data sets with many variables by which some of the variance axes may be great, whereas others may be small, such that they can be ignored (Burger and Gowen, 2011).
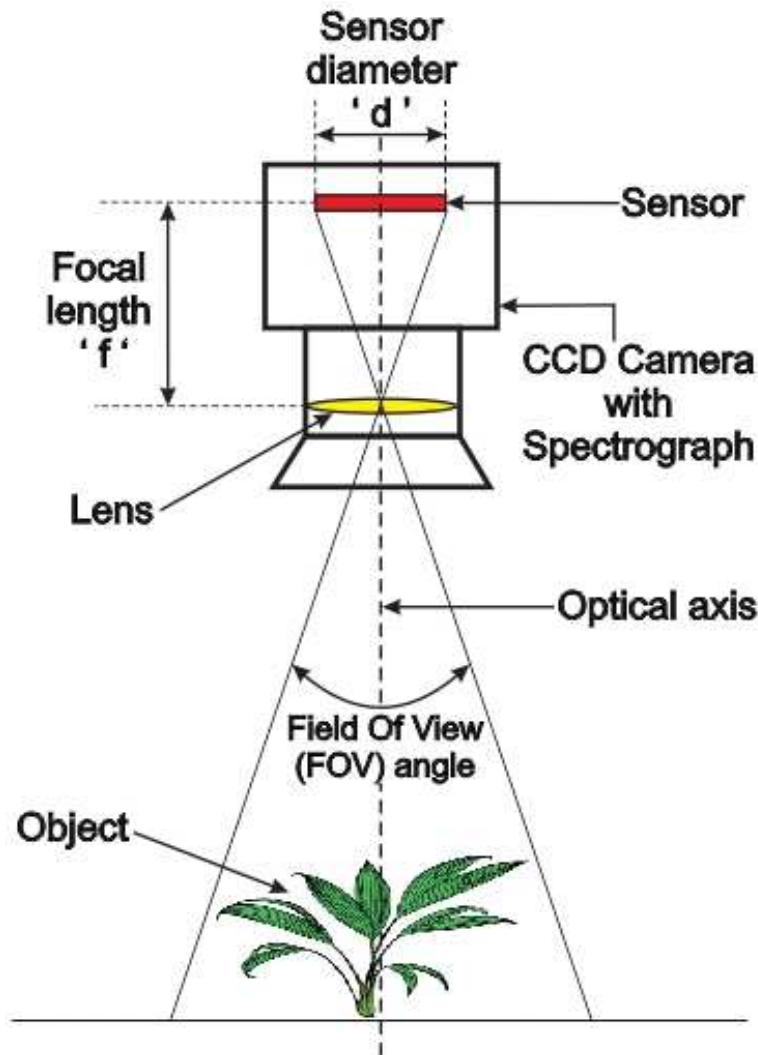
Figure 4. Hyperspectral imaging camera field of view (FOV Angle) covered an object. Where by 'f' is defined as camera focal length and 'd' as the camera sensor width or diameter.

For example one might start with 100 original variables and might end with only 10 meaningful axes. This is known as reducing the dimensionality of a data set. In this work PCA was used to reduce the spectral dimension of the hypercube images data of the tobacco leaves. The Data set (Ds) can be express as hypercube structure (λ) plus the error or noise (E), mathematically as Equation 3:

$$Ds = \lambda + E \quad = \quad (U * V * W) + E$$
(3)

Where U, V and W, are hypercube spatial axes and spectral wavelength (Figure 3b).

Minimum noise fraction (MNF) method

The minimum noise fraction transform MNF is a rotation tool that determines the inheritance dimensionality of image data, to segregate noise in the data, and to reduce the computational requirements for subsequent processing. MNF is a linear transformation that consists of separate principal components analysis rotations that includes; (i) The first rotation uses the PCs of the noise covariance matrix to decorrelate and rescale the noise in the data, (this is called noise whitening), and resulting in transformed data in which the noise has unit variance and no band-to-band correlations (Burger and Gowen, 2011). (ii) The second rotation uses the PCs derived from the original image data after they have been noise-whitened by the first rotation and rescaled by the noise standard deviation. The inherent dimensionality of the data is determined by examining the final eigenvalues and the associated images.

Also noise from the data can be removed by performing a forward transform, to examine the images and eigenvalues of bands that contain the coherent images. Then run an Inverse MNF transform using a spectral subset to include only the good bands or smoothing the noisy bands before the inverse. In ENVI, an individual end member spectra can be transformed into MNF space

for input into mixture tuned matched filtering (MTMF).

Tobacco plant diseases

Types of tobacco plant diseases

There are many types of tobacco plants disease such as foliar diseases which are related to leaves, like tobacco mosaic virus (TMV), brown spot (*Alternaria alternata*), blue mold (*Peronospora tabacina*), scab (*Hymenula affinis*) and verticillium wilt (*Verticillium albo-atrum*) (Yamaji et al., 2010; Zuo et al., 2007). Also there are soil-borne diseases like black-shank (*Phytophthora nicotianae*), granville wilt (*Ralstonia solanacearum*), root-knot nematode (*Meloidogyne arenaria*) and fusarium wilt (*Fusarium oxysporum*) (Alvessantos, 2007; Caillaud et al., 2008).

The black-shank fungus

In this experiment, the black-shank fungus (*P. nicotianae*) was used for the artificial inoculation of pot 3 and 4 tobacco plants samples. This fungus may attack tobacco plants of all ages whereby the roots and basal parts of the stem are primarily affected. The root system is often partly or completely black; a dark lesion may extend several centimeters up the stalk (Hernandez et al., 2009; Zhao et al., 2011). The infected plants usually wilt during the hottest part of the day and may not recover at the night, while the older plants infected with this disease wilt suddenly or the leaves droops. Development of this type of disease in cool weather is slower than when temperatures are high (Chacón et al., 2009). The severity levels in plants caused by the black-shank fungus can be calculated using Plant Senescence Reflectance Index (PSRI) from the hyperspectral data collected with various changes in reflectance intensity due to different infection levels (e.g. 1, 6, 12 and 18 days after inoculation in this experiment). The PSRI is designed to maximize the sensitivity of the index to the ratio of bulk carotenoids to chlorophyll (e.g. alpha-carotene and beta-carotene). An increase in PSRI indicates increased canopy stress (carotenoid pigment), the onset of canopy senescence, plant fruit ripening and so on. PSRI is defined by the Equation 4 (Brantley et al., 2011; Sankaran et al., 2010):

$$PSRI = \frac{R_{680} - R_{500}}{R_{750}} \tag{4}$$

Where PSRI is the plant senescence reflectance index, R indicates reflectance, and the subscript number indicates a particular wavelength in nm. Other studies have also indicated that it is possible through reflectance of hyperspectral imaging data to model water content and estimate the leaf drought stress when it was infested. Software such as ENVI can be used to find the specific wavelengths in which leaf reflectance was most strongly responsive to damage caused by the fungus. The water band index ratio (Equation 5) provides a good indicator of water content in the fine tissues of the canopy (Claudio et al., 2006; Sankaran et al., 2010):

$$WBI = \frac{R_{900nm}}{R_{970nm}} \tag{5}$$

Where WBI is the water band index, R_{900} and R_{970} are the leaf reflectance at wavelengths of 900 and 970 nm respectively.

RESULTS

The reflectance

The influence of the pathological status of plants on its spectral characteristics can be visible or detectable in the visible/NIR or IR regions of the electromagnetic spectrum. The spectral parameters such as single wavelength reflectance, plant senescence reflectance index (SPRI) and water band index (WBI) were used to discriminate the severity level of black-shank infection on tobacco plants. Figure 5a to d shows the average spectral images of ROIs responses over the entire spectral wavelengths (380 to 1030 nm) acquired during 1 to 18 days experiments. The ROIs from both plants during day 1 experiment shows the average spectral reflectance intensity of 73 to 75% (Figure 5a). The spectrum of plant leaves changes in both the visible/NIR regions due to physiological stress. The non-inoculated tobacco plants (pot 1 and 2) stayed healthy over the experimental period. The infected tobacco plants (pot 3 and 4) in Figure 5b day 6 experiment shows a trend similar to that of the healthy plants, but reflectance decreased slightly in both visible and the near infrared region with about 8% from day 1 experiment. At this stage no symptoms were present to the human eyes.

The differences in spectral intensities were specifically noted in both the visible and NIR regions due to the absorption of incident light changes. The reflectance of plant leaves in the visible and NIR regions decreases in advanced disease infection due to the decreased chlorophyll content, changes in other pigments and foliar internal structure (Minghua et al., 2003). The symptoms of black shank disease became visible 12 days after inoculation (DAI), whereby the leaves affected from the lower part of the plant gradually turn yellow and some hang down the stalk by 18dai. The spectra intensity of detected fluorescence determines the evaluation of disease advancement. Figure 5c and d shows the average reflectance intensity of infected plants decreases substantially to approximately 37% by 18dai compared to the day 1 spectra. While the average spectral responses of healthy plants increased slightly with about 6% throughout the experimental days.

The pathological conditions of plants, vegetation, plants disease and so on, can be recognized visibly or detectable either within visible/NIR or IR regions of electromagnetic spectrum range. The spectrums of green plants are determined by their chemical and morphological characters, which have a close relation to growth periods, health conditions and seasonal phenomenon (Yang et al., 2000). The obtained spectral characteristics of fluorescence with intensity peaks in 521 to 650 nm (116 to 220 bands), and 720 to 850 nm (275 to 376 bands) range, were sensitive to the black-shank severity level, also explicitly outlined healthy and pathologically changed areas. But specifically the wavelengths of 730 and 790 nm
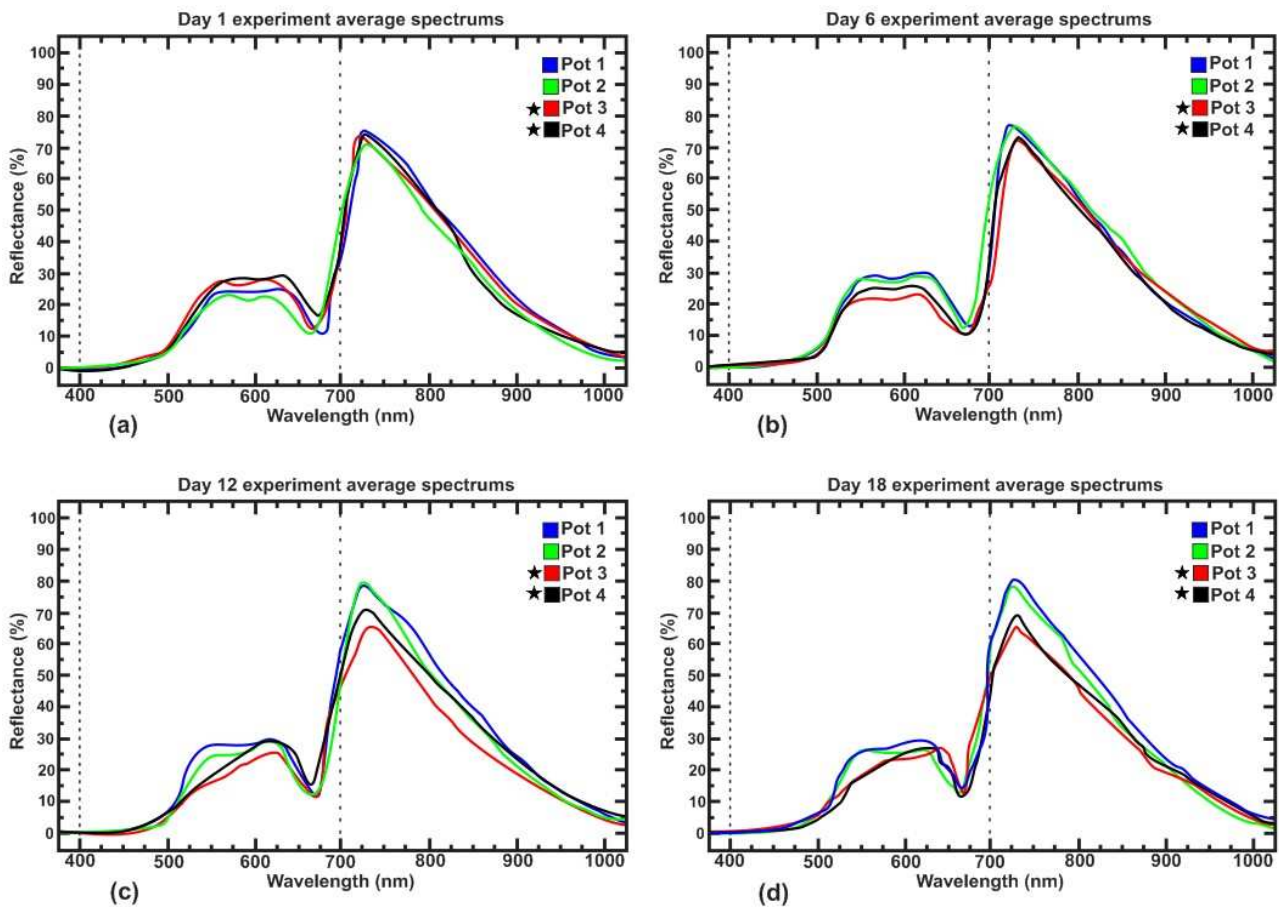
Figure 5. Average spectrums of tobacco plants pots regions of interest (ROIs). Where (a) is day 1 experiment average spectra, (b) is day 6 experiment average spectra, (c) is day 12 experiment average spectra and (d) is day 18 experiment average spectra. The pot 3 and 4 with star symbols are the inoculated pots with black-shank disease which was immediately after day 1 experiment. The inoculated pots average spectral reflectance from day 6 to 18 decreases significantly with the increasing severity level at both the visible and near-infrared wavelength ranges. While the average Spectral of healthy plants pot 1 and 2 increased slightly with about 5% throughout the experimental days.

with corresponding bands of 283 and 330 provided the highest correlation coefficient.

The moisture of the tobacco leaves

When the plants are stressed by the disease, the water content and absorption of incident light of that plants changes in both the visible and near infrared range. This reaction is probably due to the decreased chlorophyll content, changes in other pigments and foliar internal structure (Minghua et al., 2003).The agricultural stress tool and vegetation index calculator in ENVI was used to analyze the leaf moisture content from hyperspectral reflectance data. These tools are intended specifically for use on agricultural product and agricultural land to support precision agriculture analysis, to designed and create a spatial map showing the distribution of crop stress. The crops or plants exhibiting low stress conditions

is usually made up of healthy vegetation, while the plants under high stress conditions shows signs of dry or dying plant material, very dense or sparse canopy, and inefficient light use (Brantley et al., 2011).

Both the agricultural stress tool and vegetation index calculator uses vegetation indices (VIs) that are constructed from reflectance measurements in two or more wavelengths in order to analyse specific characteristics of vegetation, such as total leaf area and water content. Table 1 shows some indices equations grouped into categories that calculate similar properties, and their functions in field of analysis (Kim et al., 2011; Sankaran et al., 2010). The tobacco plants water contents were analyzed using agricultural stress tool by which three of VIs bands was selected from each category at a time. The selected VIs bands include; (i) normalized difference vegetation index (NDVI) from broadband greenness category (ii) photochemical reflectance index (PRI) from light use efficiency category and (iii) water band index

Table 1. The Vegetation Indices (VIs) grouped into categories that calculate similar properties. VIs are combinations of surface reflectance at two or more wavelengths designed to highlight a particular property of vegetation. Each of the VIs is designed to accentuate a particular vegetation property.

VIs Cat.	Indices group	Description	Equation	Reference
Broadband greenness	Normalized Difference Vegetation Index (NDVI)	Is one of the oldest, most well-known, and most frequently used VIs. Its formulation and use of the highest absorption and reflectance regions of chlorophyll make it robust over a wide range of conditions.	$NDVI = \dfrac{R_{800} - R_{670}}{R_{800} + R_{670}}$	(Brantley et al., 2011)
	Enhanced Vegetation Index (EVI)	An enhancement on the NDVI to better account for soil background and atmospheric aerosol effects.	$EVI = 2.5 \left(\dfrac{R_{800} - R_{680}}{R_{800} + 6R_{680} - 7.5R_{450} + 1} \right)$	(Kim et al., 2011)
	The Simple Ratio (SR) index	The SR is the ratio of the highest reflectance; absorption bands of chlorophyll makes it both easy to understand and effective over a wide range of conditions	$SR = \dfrac{R_{801}}{R_{670}}$	(Daughtry et al., 2000)
	Atmospherically Resistant Vegetation Index (ARVI)	Is an enhancement to the NDVI that is relatively resistant to atmospheric factors (for example, aerosol). It uses the reflectance in blue to correct the red reflectance for atmospheric scattering	$ARVI = \dfrac{R_{800} - (2 * R_{680} - R_{450})}{R_{800} + (2 * R_{680} - R_{450})}$	(Kim et al., 2011)
Narrowband greenness	The Modified Red Edge Normalized Difference Vegetation Index (mNDVI$_{705}$)	Is a modification of the Red Edge NDVI, it capitalizes on the sensitivity of the vegetation red edge to small changes in canopy foliage content, gap fraction, and senescence.	$mNDVI_{705} = \dfrac{R_{750} - R_{705}}{R_{750} + R_{705} - 2R_{445}}$	(Daniel and John, 2002)
	The Vogelmann Red Edge Index 1 (VOG1)	A narrowband reflectance measurement that is sensitive to the combined effects of foliage chlorophyll concentration, canopy leaf area, and water content.	$VOG1 = \dfrac{R_{740}}{R_{720}}$	(Kim et al., 2011)
	Vogelmann Red Edge Index (VOG 2 & 3). In VOG3 it is R$_{720}$ in place of R$_{726}$	A shape of the near-infrared transition that is indicative of the onset of canopy stress and senescence.	$VOG2 = \dfrac{R_{734} - R_{747}}{R_{715} + R_{726}}$	(Kim et al., 2011)
Light use efficiency	Photochemical Reflectance Index (PRI)	Useful to estimate absorption by leaf carotenoids (especially xanthophyll) pigments, leaf stress, and carbon dioxide uptake.	$PRI = \dfrac{R_{531} - R_{570}}{R_{531} + R_{570}}$	(Huang et al., 2007)
	Structure Insensitive Pigment Index (SIPI)	Indicator of leaf pigment concentrations normalized for variations in overall canopy structure and foliage content.	$SIPI = \dfrac{R_{800} - R_{445}}{R_{800} - R_{680}}$	(Rumpf et al., 2010)
Dry or senescent	Cellulose Absorption Index (CAI)	A vegetation index indicating exposed surfaces containing dried plant material.	$CAI = 0.5(R2000 + R2200) - R2100$	(Daughtry et al., 2004)
	Plant Senescence Reflectance Index (PSRI)	Uses a ratio of carotenoids to chlorophyll to detect onset and degree of plant senescence.	$PSRI = \dfrac{R_{680} - R_{500}}{R_{750}}$	(Kim et al., 2011)
Leaf pigments	Carotenoid Reflectance Index (CRI1 & 2). In CRI2, it is R$_{700}$ in place of R$_{500}$	Detects a relative difference in absorption indicative of changes in leaf total carotenoid concentration relative to chlorophyll concentration.	$CRI1 = \left(\dfrac{1}{R_{510}} \right) - \left(\dfrac{1}{R_{550}} \right)$	(Anatoly et al., 2002)
	Anthocyanin Reflectance Index (ARI1 & 2). In ARI1, there is no R$_{800}$ wavelength	A variant of the ARI1, which is sensitive to changes in GREEN absorption relative to RED, indicating leaf anthocyanins.	$ARI2 = R_{800} \left[\left(\dfrac{1}{R_{550}} \right) - \left(\dfrac{1}{R_{700}} \right) \right]$	(Anatoly et al., 2001)

Table 1. Contd.

Canopy water content	Water Band Index (WBI)	Reflectance measurement that is sensitive to changes in canopy water status	$WBI = \dfrac{R_{900\,nm}}{R_{970\,nm}}$	(Sankaran et al., 2010)
	Moisture Stress Index (MSI)	Reflectance measurement that is sensitive to increasing or decrease of leaf water content	$MSI = \dfrac{R_{1599}}{R_{819}}$	(Pietro et al., 2001)
	Normalized Difference Infrared Index (NDII)	A reflectance measurement that is sensitive to changes in water content of plant canopies. It uses a normalized difference formulation instead of a simple ratio.	$NDII = \dfrac{R_{819} - R_{1649}}{R_{819} + R_{1649}}$	(Jackson, 2004)

Source of categorization: ENVI manual and tutorial DVD shipped with software.

(WBI) from canopy water-content category (Table 1).

The vegetation index calculator provides 27 predefined VIs that can be used to detect the presence and relative abundance of various vegetation properties from hyperspectral data. These VIs are combinations of surface reflectance at two or more wavelengths designed to highlight a particular property of vegetation. Each index is grouped into a category by the main function of the index (Sonnentag, 2008). The 'biophysical cross checking' which is one of the truly unique features for the vegetation analysis component in ENVI was set to be 'On' from the VIs calculator parameters window. If enabled, allows the comparison of different indices at each pixel to validate their results. All or some of the available VIs appears in the calculator can be selected and click OK to passed the result into the available bands list window. Figure 6a and b shows the ENVI vegetation index calculator, and available bands list window for pot 3 tobacco plants data respectively.

Results can be loaded in gray-scale by selecting one band of VIs at a time, or loaded in RGB colors by selecting 3 bands of VIs at a time and fill them in R, G and B columns in available bands list window (Figure 6b). Figure 7 compared the results in RGB colors of moisture contents for figure 7a healthy tobacco leaf from pot 3 during day 1 experiments, and Figure 7b which shows the same leaf infected 18dai with black-shank. The color ramp displayed the classes whereby blue to green represent low stress (that is, healthy plants or vegetation), whereas yellow to reds indicate high stress (that is, weakest / infected plants or vegetation).

Based on our results obtained, the decrease in reflectance is indicating the increase in severity level. Figure 8 shows the stress plot of healthy and infected tobacco plants disease advancements in percentages. The infected plant shows the disease advancement of about 37% by 18dai. While non-inoculated plants increased in reflectance with about 6% and stayed healthy throughout the experimental days. The percentage calculations are based on reduced and increased of the average spectra from day 1 to 18 experiments.

Principal component analysis (PCA)

Principal component analysis (PCA) was used to find the overall similarities and differences of healthy and infected tobacco plants within 380 to 1030 nm wavelength. The average reflectance spectra obtained from day 18 final experiment for both healthy and infected tobacco plants pots samples was used. The collected spectrum which was represents the average area of the samples plants, showed similarity in patterns but differ on the reflectance absolute values. In order for the PCA to work properly, the mean was subtracted from each of the data dimensions which produce the data set whose mean is equal to zero. Then the data was transferred to the "unscrambler" Statistical Analysis software by (CAMO software AS), for PCA.

The first derivatives obtained from the average reflectance show that the most important wavelength are identified at 630, 680, 750, 790, 840 and 880 nm. The first three principal components from the variance curve generated they were responsible for 94.8% of variability of the data. The 1st, 2nd and 3rd variability are 80.4, 12.2 and 2.2%, respectively. Figure 9 shows PCA scores plot of the afore-mentioned selected wavelength whereby almost all the high reflectance of pot 1 and 2 samples pots (non-inoculated plants) are located in the positive area of both PC1 and PC2. The sample plants from pot 3 and 4 (inoculated plants) are almost entirely located in the negative area indicating inverse relationship among these two quality classes, whereas the scores located at the center are medium reflectance region from both of the pots.

DISCUSSION

The results of this study demonstrate the potential application of hyperspectral remote sensing within 380 to 1030 nm wavelength, as a rapid and field based method of identifying healthy and infected plants prior to symptom expression, with overall accuracy of 90 to 94% from both
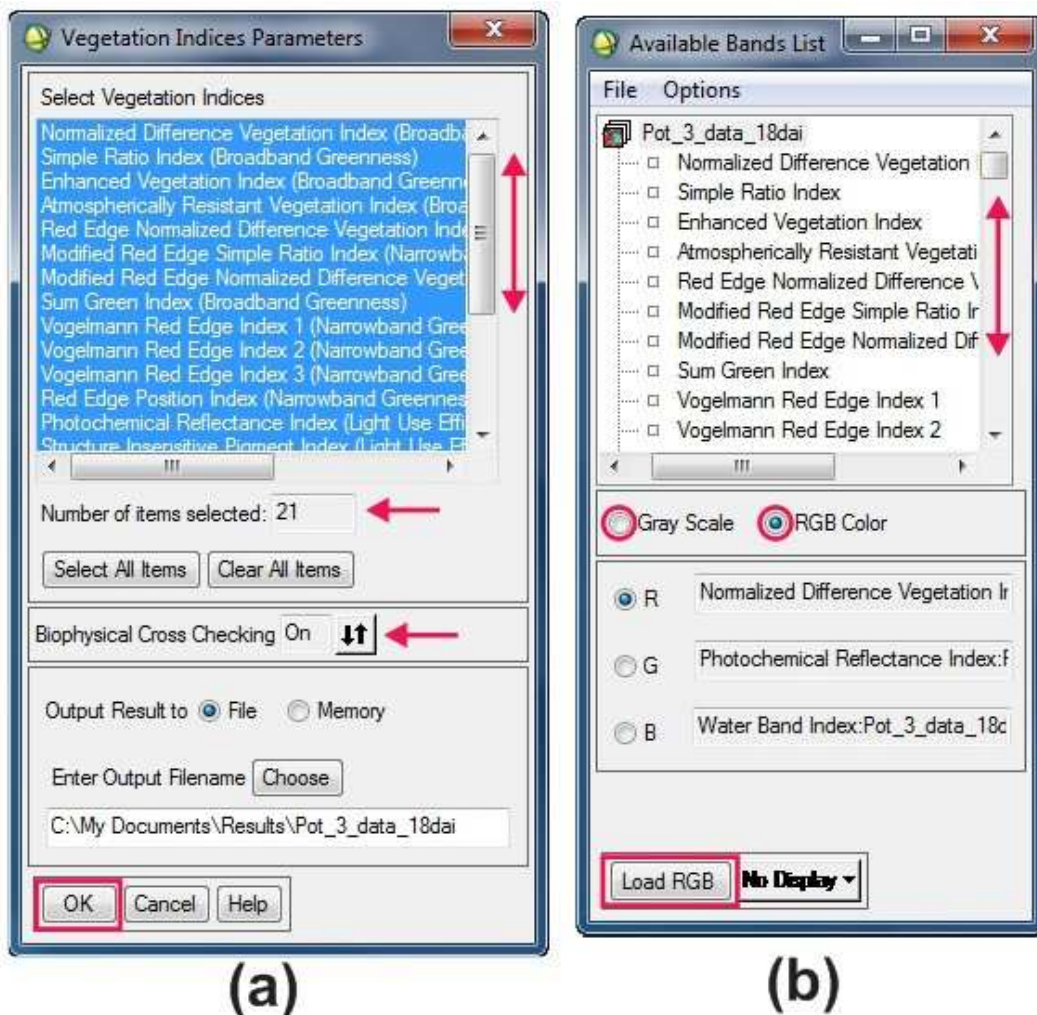
Figure 6. ENVI predefined indices. Where (a) is ENVI Vegetation indices calculator showing 21 available indices that can be calculated from pot 3 tobacco plants samples at 18dai out of 27 predefined VIs by ENVI. (b) Is the available bands list window which appears after selecting indices and clicking OK from indices calculator. Results can be loaded in gray-scale by selecting one band of VIs at a time, or loaded in RGB colours by selecting 3 bands of VIs at a time and fill them in R, G and B columns in available bands list window.

indices and the PCA. Disease can be detected within first six days of development after infection even if the symptoms cannot be visibly seen by the human eye, so that action can be taken as soon as possible. The spectral range from 520 to 650 nm (116 to 220 bands), and 720 to 850 nm (275 to 376 bands) was useful for discriminating black-shank fungus severity levels, especially at the wavelength of 730 nm (283 band) and 790 nm (330 band), where the differences in reflectance between levels were the largest. These results are in agreement with findings obtained by (Daughtry et al., 2004; Muhammed, 2002; Naidu et al., 2009; Xu et al., 2007) for spectral reflectance decreases significantly with the increasing severity level at both the visible and near-

infrared wavelength ranges. While (Minghua et al., 2003) reported that if a plant is infected the spectral reflectance increases in the visible region and decreases within NIR region.

Although this experiment was performed in laboratory, but the application of hyperspectral remote sensing for disease detection already applied on many crops both under field conditions, larger plantations and in greenhouses. In this work for example, more than 30 references are based on hyperspectral applications in which 21 of them are laboratory experiments, (Laudien et al., 2005) used hyperspectral sensor integrated with tractor-based for detection of plants stress under field condition, and (Kim et al., 2011) hang-up on roof of the
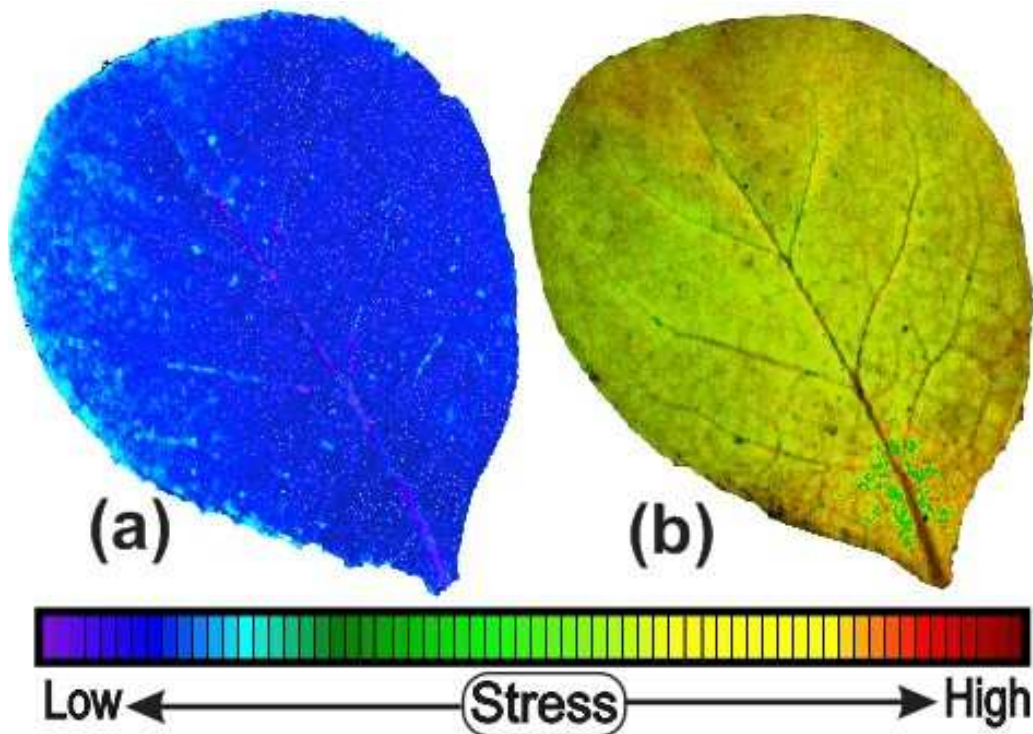
Figure 7. RGB colors of moisture contents of (a) healthy tobacco leaf during day 1 experiment and (b) shows the same tobacco leaf by 18 days after inoculation with black-shank disease. The colour ramp displayed the classes whereby blue to green represent low stress (that is, healthy plants or vegetation), whereas yellow to reds indicate high stress (that is, weakest / infected plants or vegetation).

greenhouse the hyperspectral imaging to monitor the crop changes. While (Brantley et al., 2011; Daughtry et al., 2004; Naidu et al., 2009; Rumpf et al., 2010) used portable hyperspectral for detection of crops diseases under field conditions, and (Freek, 2004; Glaber et al., 2011; Huang et al., 2007; Jackson, 2004; Minghua et al., 2003; Plaza et al., 2009; Xu et al., 2008) used hyperspectral imaging installed on satellites and aircrafts such as Landsat 7, Landsat 5TM, Landsat ETM+, TRWIS III Airborne, German Digital Airborne and NASA's Airborne Visible-Infrared Imaging Spectrometer (AVIRIS) for crops disease detections under field conditions.

Hyperspectral vision systems work by using devices that are capable of filtering incident electromagnetic radiation and transmitting only that corresponding to a specific wavelength, depending on the technology they employed. These devices can be classified into imaging spectrometers like acousto-optical tunable filters (AOTF) and liquid crystal tunable filters (LCTF), used in such as ImSpector Spectrographs and airborne hyperspectral imaging systems (Gomezsanchis et al., 2008). As applied to the field of optical remote sensing such as crop disease detection, spectrograph deals with the spectrum of sunlight that is diffusely reflected (scattered) by materials at the earth's surface. Although the weather condition (e.g. solar lighting) and the leaves inclination

imply a multiplicative effect and an additive effect on the obtained reflectance (Vigneau et al., 2011), but the overall shape of a spectral curve, the position and strength of absorption bands in many cases can be used to identify and discriminate different materials. Where by each pixel contain a unique, continuous spectrum for the identification of terrestrial materials by their reflectance after atmospheric correction. The hyperspectral imaging still remains valuable technique for detection and classification of materials and objects on the earth's surface.

Conclusion

Hyperspectral imaging has a great potential on non-destructive testing technology, also is a real-time system capable of discriminating between stressed and non-stressed plants. This study proved the feasibility of early detection of black-shank disease on tobacco plants. The reflectance differences between healthy and infected tobacco plants samples were found within visible/NIR wavelength regions (380 to 1030 nm). However, using hyperspectral imaging to determine severity of plant diseases may improve to make good use of the pesticide, only applying when and where needed and reducing the
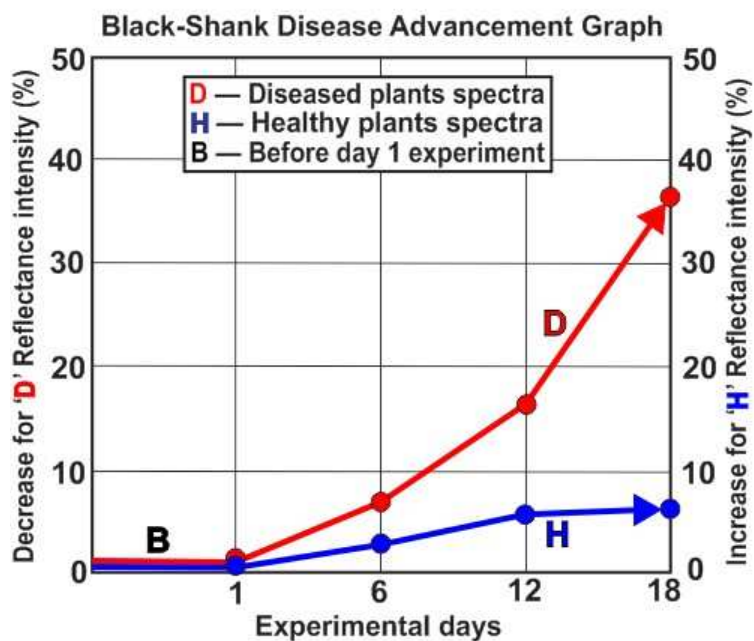
Figure 8. Stress plot of healthy and infected tobacco plants disease advancements. Percentage by the left side shows the disease advancement of infected plants 'D' to about 37% by 18dai. While percentage by the right side shows non-inoculated plants 'H' stayed healthy with increase in reflectance of about 6% throughout the experimental period. 'B' is the average spectra of both plants before day 1 experiment. Based on our results, the decrease in reflectance is indicating the increase in severity level. The calculations are based on the average spectra reduced and increased from day 1 to 18 experiments.
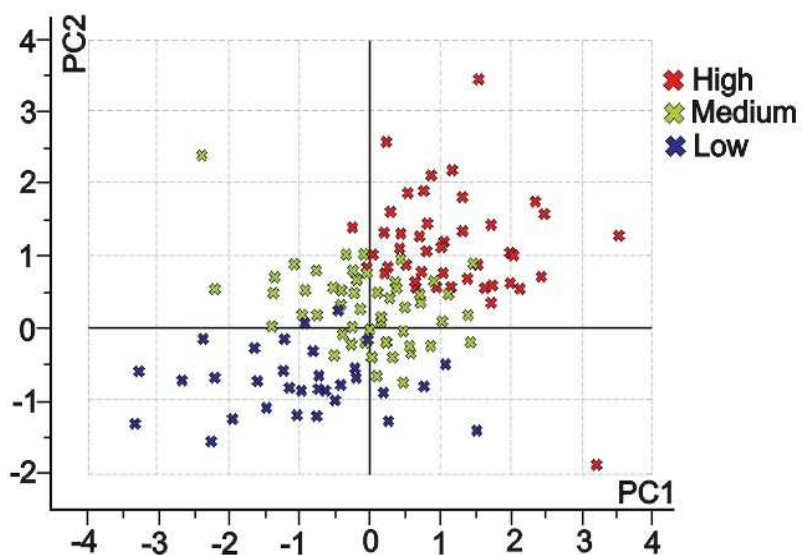

Figure 9. Principal Components Analysis Scores plot. The healthy plants (pot 1 and 2) are located in the positive area of both PC1 and PC2 with high reflectance. While the inoculated plants (pot 3 and 4) are almost entirely located in the negative area with low reflectance indicating inverse relationship among these two quality classes, whereas the scores located at the center are medium reflectance regions from both of the pots.

residues in produce and environmental contamination.

REFERENCES

Alvessantos F (2007). Cultural characteristics, pathogenicity and genetic diversity of *Fusarium oxysporum* isolates from tobacco fields in Spain. Physiol. Mol. Plant Pathol., 71: 26-32.

Anatoly AG, Mark NM, Olga BC (2001). Optical Properties and Nondestructive Estimation of Anthocyanin Content in Plant Leaves. Photochem. Photobiol., 74(1): 38-45.

Anatoly AG, Yoav Z, Olga BC, Mark NM (2002). Assessing Carotenoid Content in Plant Leaves with Reflectance Spectroscopy. Photochem. Photobiol., 75(3): 272-281.

Bauriegel E, Giebel A, Herppich WB (2011). Hyperspectral and Chlorophyll Fluorescence Imaging to Analyse the Impact of *Fusarium culmorum* on the Photosynthetic Integrity of Infected Wheat Ears. Sensors, 11(4): 3765-3779.

Brantley ST, Zinnert JC, Young DR (2011). Application of hyperspectral vegetation indices to detect variations in high leaf area index temperate shrub thicket canopies. Rem. Sens. Envron., 115(2): 514-523.

Burger J, Gowen A (2011). Data handling in hyperspectral image analysis. Chem. Int. Lab. Syst., 108(1): 13-22.

Caillaud MC, Dubreuil G, Quentin M, Perfus BL, Lecomte P, Almeida EJ, Abad P, Rosso MN, Favery B (2008). Root-knot nematodes manipulate plant cell functions during a compatible interaction. Plant Physiol. J., 165(1): 104-113.

Chacón O, Hernández I, Portieles R, López Y, Pujol M, Borrás-Hidalgo O (2009). Identification of defense-related genes in tobacco responding to black shank disease. Plant Sci., 177(3): 175-180.

Ciaran H, Patrick D, Edward J, Martin G (2010). Accuracy of fish-eye lens models. Appl. Optics, 49(17): 3338-3347.

Claudio H, Cheng Y, Fuentes D, Gamon J, Luo H, Oechel W, Qiu H, Rahman A, Sims D (2006). Monitoring drought effects on vegetation water content and fluxes in chaparral with the 970 nm water band index. Rem. Sens. Environ., 103(3): 304-311.

Daniel AS, John AG (2002). Relationships between leaf pigment content and spectral reflectance across a wide range of species, leaf structures and developmental stages. Rem. Sens. Environ., 81: 337-354.

Daughtry CST, Hunt ER, McMurtrey JE (2004). Assessing crop residue cover using shortwave infrared reflectance. Rem. Sens. Environ., 90(1): 126-134.

Daughtry CST, Walthall CL, Kim MS, Brown DC, McMurtrey JE (2000). Estimating corn leaf chlorophyll concentration from leaf and canopy reflectance. Remote Sens. Envron., 74: 229-239.

Dian P, Andueza D, Jestin M, Prado I, Prache S (2008). Comparison of visible and near infrared reflectance spectroscopy to discriminate between pasture-fed and concentrate-fed lamb carcasses. Meat Sci., 80(4): 1157-1164.

Freek VDM (2004). Analysis of spectral absorption features in hyperspectral imagery. Int'l. J. Appl. Earth Observ. Geoinf., 5(1): 55-68.

Garcia APB, Conde OM, Mirapeix J, Cobo A, Lopez HJM (2008). Quality control of industrial processes by combining a hyperspectral sensor and Fisher's linear discriminant analysis. Sens. Actua., 129(2): 977-984.

Glaber C, Groth D, Frauendorf J (2011). Monitoring of hydrochemical parameters of lignite mining lakes in Central Germany using airborne hyperspectral casi-scanner data. Int. J. Coal Geo., 86(1): 40-53.

Gomezsanchis J, Molto E, Campsvalls G, Gomezchova L, Aleixos N, Blasco J (2008). Automatic correction of the effects of the light source on spherical objects. An application to the analysis of hyperspectral images of citrus fruits. Food Engr. J., 85(2): 191-200.

Grisham MP, Johnson RM, Zimba PV (2010). Detecting Sugarcane yellow leaf virus infection in asymptomatic leaves with hyperspectral remote sensing and associated leaf pigment changes. Virologic. Methods J., 167(2): 140-145.

Hernandez I, Chacon O, Rodriguez R, Portieles R, Lopez Y, Pujol M, Borras HO (2009). Black shank resistant tobacco by silencing of glutathione S-transferase. Biochem. Biophys. Res. Comm., 387(2): 300-304.

Huang W, Lamb DW, Niu Z, Zhang Y, Liu L, Wang J (2007). Identification of yellow rust in wheat using *in-situ* spectral reflectance measurements and airborne hyperspectral imaging. Prec. Agric., 8: 187-197.

Jackson T (2004). Vegetation water content mapping using Landsat data derived normalized difference water index for corn and soybeans. Rem. Sens. Environ., 92(4): 475-482.

Jinsung P, Seong JJ, Songcheol H, Jong IS (2002). Reduction of dark current in an n-type In0.3Ga0.7As/GaAs quantum well infrared photodetector by using a camel diode structure. Solid-State Electr., 46: 651-654.

Kim Y, Glenn DM, Park J, Ngugi HK, Lehman BL (2011). Hyperspectral image analysis for water stress detection of apple trees. Compt. Electr. Agric., 77(2): 155-160.

Laudien R, Bareth G, Doluschitz R (2005). Multitemporal hyperspectral data analysis for regional detection of plant stress by using an airborne- and tractor-based spectrometer. Visual Communications and Image Processing (VCIP), Computer Vision and Modeling Commission V - Close-Range Sensing, Analysis and Applications, International Society for Photogrammetry and Remote Sensing (ISPRS), Beijing, China, 2005, July 12-15, pp. 1-5.

Minghua Z, Zhihao Q, Xue L, Susan LU (2003). Detection of stress in tomatoes induced by late blight disease in California, USA, using hyperspectral remote sensing. Intl. J. Appl. Earth Observ. Geoinf., 4(4): 295-310.

Muhammed HH (2002). Using Hyperspectral Reflectance Data for Discrimination between Healthy and Diseased Plants, and Determination of Damage-Level in Diseased Plants. IEEE Proceedings of the 31st Applied Imagery Pattern Recognition Workshop, 16-17 October, 2002; pp. 49-54.

Muhammed HH (2005). Hyperspectral Crop Reflectance Data for characterising and estimating Fungal Disease Severity in Wheat. Biosys. Engr., 91(1): 9-20.

Naganathan G, Grimes L, Subbiah J, Calkins C, Samal A, Meyer G (2008). Visible/near-infrared hyperspectral imaging for beef tenderness prediction. Compt. Electr. Agric., 64(2): 225-233.

Naidu AR, Perry EM, Pierceb FJ, Mekuria T (2009). The potential of spectral reflectance technique for the detection of Grapevine leafroll-associated virus-3 in two red-berried wine grape cultivars. Compt. Electr. Agric., 66(1): 38-45.

Pietro C, Stephane F, Stefano T, Stephane J, Jean MG (2001). Detecting vegetation leaf water content using reflectance in the optical domain. Rem. Sens. Environ., 77: 22-33.

Plaza J, Plaza AJ, Barra C (2009). Multi-Channel Morphological Profiles for Classification of Hyperspectral Images Using Support Vector Machines. Sensors, 9(1): 196-218.

Rumpf T, Mahlein AK, Steiner U, Oerke EC, Dehne HW, Plümer L (2010). Early detection and classification of plant diseases with Support Vector Machines based on hyperspectral reflectance. Compt. Elect. Agric., 74(1): 91-99.

Sankaran S, Mishra A, Ehsani R, Davis C (2010). A review of advanced techniques for detecting plant diseases. Compt. Electr. Agric., 72(1): 1-13.

Singh CB, Jayas DS, Paliwal J, White NDG (2009). Detection of insect-damaged wheat kernels using near-infrared hyperspectral imaging. Stored Prod. Res. J., 45(3): 151-158.

Sonnentag O (2008). Image Analysis, Classification and Change Detection in Remote Sensing With Algorithms for ENVI/IDL. Compt. Geosci., 34(1): 93-94.

Vigneau N, Ecarnot M, Rabatel G, Roumet P (2011). Potential of field hyperspectral imaging as a non destructive method to assess leaf nitrogen content in Wheat. Field Crops Res., 122(1): 25-31.

Xu H, Ying Y, Fu X, Zhu S (2007). Near-infrared Spectroscopy in detecting Leaf Miner Damage on Tomato Leaf. Biosys. Engr., 96(4): 447-454.

Xu W, Wooster MJ, Grimmond CSB (2008). Modelling of urban sensible heat flux at multiple spatial scales: A demonstration using airborne hyperspectral imagery of Shanghai and a temperature–emissivity separation approach. Rem. Sens. Environ., 112(9): 3493-3510.

Yamaji Y, Hamada K, Yoshinuma T, Sakurai K, Yoshii A, Shimizu T, Hashimoto M, Suzuki M, Namba S, Hibi T (2010). Inhibitory effect on the tobacco mosaic virus infection by a plant RING finger protein. Virus Res., 153(1): 50-57.

Yang H, Zhang J, Van DMF, Kroonenberg SB (2000). Spectral characteristics of wheat associated with hydrocarbon microseepages. Int'l J. Remote Sens., 20(4): 807-813.

Yongliang L, Yudren C, Chien YW, Diane EC, Moon SK (2005). Development of a simple algorithm for the detection of chilling injury in cucumbers from visible/near-infrared hyperspectral imaging. Appl. Spectros., 59(1): 78-85.

Zhao F, Zhao ZX, Xu FH, Duan FY, Lufen ZK, Wang DX, Yang HW, Xu XY (2011). Effect of nitrogen application rate on physiology of flue-cured tobacco plants with or without inoculation of Phytophthora parasitica var. nicotianae and the severity of black shank. Plant Nutr. Fert. Sci., 17(3): 737-743.

Zuo KJ, Qin J, Zhao JY, Ling H, Zhang LD, Cao YF, Tang KX (2007). Over-expression GbERF2 transcription factor in tobacco enhances brown spots disease resistance by activating expression of downstream genes. Gene, 391: 80-90.